

**Evaluation of potential variations around grain boundaries in BaSi<sub>2</sub> epitaxial films by Kelvin probe force microscopy**

Masakazu Baba, Sadahiro Tsurekawa, Kentaro Watanabe, W. Du, Kaoru Toko, Kosuke O. Hara, Noritaka Usami, Takashi Sekiguchi, and Takashi Suemasu

Citation: *Applied Physics Letters* **103**, 142113 (2013); doi: 10.1063/1.4824335

View online: <http://dx.doi.org/10.1063/1.4824335>

View Table of Contents: <http://scitation.aip.org/content/aip/journal/apl/103/14?ver=pdfcov>

Published by the [AIP Publishing](#)

---

An advertisement for Integrated Engineering Software. It features a yellow background with a grid of dotted lines. On the left, there is a logo consisting of a blue square with a white dot pattern. To the right of the logo, the text 'INTEGRATED ENGINEERING SOFTWARE' is written in a bold, blue, sans-serif font. Below this, the text 'Particle and Beam Ray Tracing Simulation' is written in a dark grey font, followed by 'Send us your model and see LORENTZ in action' in a smaller, dark grey font. On the right side, there is a 3D visualization of a particle or beam simulation, showing a red beam entering a blue and green structure. At the bottom right, the text 'LEARN MORE' is written in a white, bold, sans-serif font, slanted upwards.

## Evaluation of potential variations around grain boundaries in BaSi<sub>2</sub> epitaxial films by Kelvin probe force microscopy

Masakazu Baba,<sup>1</sup> Sadahiro Tsurekawa,<sup>2</sup> Kentaro Watanabe,<sup>1</sup> W. Du,<sup>1</sup> Kaoru Toko,<sup>1</sup> Kosuke O. Hara,<sup>3</sup> Noritaka Usami,<sup>3,4</sup> Takashi Sekiguchi,<sup>5</sup> and Takashi Suemasu<sup>1,4</sup>

<sup>1</sup>*Institute of Applied Physics, University of Tsukuba, Ibaraki 305-8573, Japan*

<sup>2</sup>*Graduate School of Science and Technology, Kumamoto University, Kumamoto 860-8555, Japan*

<sup>3</sup>*Graduate School of Engineering, Nagoya University, Chikusa-ku, Nagoya 464-8603, Japan*

<sup>4</sup>*Japan Science and Technology Agency, CREST, Chiyoda-ku, Tokyo 102-0075, Japan*

<sup>5</sup>*National Institute for Materials Science, Ibaraki 305-0044, Japan*

(Received 9 August 2013; accepted 20 September 2013; published online 3 October 2013)

Potential variations around the grain boundaries (GBs) on the surface in undoped *n*-BaSi<sub>2</sub> epitaxial films on Si(111) and Si(001) were analyzed using Kelvin probe force microscopy. The potentials were higher at GBs than those in the BaSi<sub>2</sub> grains on Si(111). The average barrier height was approximately 30 meV at the GBs, indicating that the enhanced potentials repulse photogenerated holes so that the charge carrier recombination can be effectively reduced. In contrast, the potentials were smaller at GBs in the BaSi<sub>2</sub> on Si(001), and the average barrier heights were approximately 30 and 50 meV along Si[1–10] and [110], respectively. © 2013 AIP Publishing LLC. [<http://dx.doi.org/10.1063/1.4824335>]

Grain boundaries (GBs) and other defects in a film often deteriorate electrical and optical properties of the film. Therefore, a lot of studies have been carried out on GBs in solar cell materials such as polycrystalline Si and chalcopyrite semiconductors to improve efficiency.<sup>1–10</sup> At the same time, intensive efforts have been exerted to explore different materials other than Si, Cu(In,Ga)Se<sub>2</sub>, and III-V compound semiconductors. We have specifically targeted realizing *pn* junction solar cells using semiconducting barium disilicide (BaSi<sub>2</sub>). Composed of earth-abundant elements, BaSi<sub>2</sub> has a band gap of approximately 1.3 eV, and a large absorption coefficient reaching  $3 \times 10^4 \text{ cm}^{-1}$  at 1.5 eV.<sup>11,12</sup> Recent experimental results on large photoresponsivity, long minority-carrier lifetime, and conductivity control by impurity doping in the undoped *n*-BaSi<sub>2</sub> have spurred interest in this material.<sup>13–17</sup> In particular, the minority-carrier diffusion length, a key parameter determining the performance of solar cells, was found to be approximately 10 μm in the undoped *n*-BaSi<sub>2</sub> epitaxial film on Si(111) by means of an electron-beam-induced current technique.<sup>18</sup> This value is much larger than the grain size of the BaSi<sub>2</sub> (~0.2 μm), implying that the GBs do not work as defect centers for minority carriers (holes) in *n*-BaSi<sub>2</sub>. However, there have been no reports thus far on the GBs in BaSi<sub>2</sub>. Kelvin probe force microscopy (KFM) is considered one of the most powerful methods for evaluating GB character from the viewpoint of potential variations. For polycrystalline Si and compound semiconductors, GBs character was discussed in detail from the view points of band lineup and barrier height around the GBs using KFM.<sup>19–22</sup> In this study, we analyzed potential variations and barrier heights around the GBs in BaSi<sub>2</sub> epitaxial films both on Si(111) and Si(001) substrates using KFM.

An ion-pumped molecular beam epitaxy (MBE) system equipped with a standard Knudsen cell for Ba and an electron-beam evaporation source for Si was used. *a*-Axis-oriented undoped *n*-BaSi<sub>2</sub> epitaxial layers were grown on Si(111), sample A, and on Si(001), sample B. The BaSi<sub>2</sub> layer thicknesses were 100 and 400 nm, respectively. The

details of the growth procedure are described elsewhere.<sup>23,24</sup> Surface topographies and electrostatic potential variations were investigated using Shimadzu 9600 atomic force microscopy (AFM) and KFM, respectively. Plan-view transmission electron microscopy (TEM) images were observed using TOPCON EM-002B with the acceleration voltage being 120 kV in order to investigate the grain size of BaSi<sub>2</sub> and GBs. Samples were prepared by mechanical polishing and ion milling.

Figures 1(a) and 1(b) show the plan-view bright-field (BF) TEM images of *a*-axis-oriented BaSi<sub>2</sub> films on Si(111) and Si(001), respectively. The incident electron beam was almost parallel to the BaSi<sub>2</sub>[100] zone axis, but it was slightly tilted for the GBs to be seen clearly. According to previous studies,<sup>18,23–25</sup> *a*-axis-oriented BaSi<sub>2</sub> multi-domain epitaxial films formed on Si(111) and Si(001) surfaces have three and two epitaxial variants rotated by 120° and 90° with each other, respectively, around the surface normal. In Fig. 1(a), we see that approximately 60° and 120°, sharp GBs are present, and these GBs consist mostly of BaSi<sub>2</sub>(011) and (0-11) planes. Detailed discussions about the GBs were given in our previous report.<sup>18</sup> In the case of BaSi<sub>2</sub> on Si(001), various types of GBs are likely to exist. Among them, straight-line GBs running along the Si[110] appear dominant as shown in Fig. 1(b), and these GBs consist mostly of BaSi<sub>2</sub>(001) planes. The epitaxial relationship between BaSi<sub>2</sub> and Si(001) is BaSi<sub>2</sub>(100)//Si(001) with BaSi<sub>2</sub>[010]//Si[110] (variant A) and BaSi<sub>2</sub>[001]//Si[110] (variant B) for BaSi<sub>2</sub> on Si(001).<sup>25</sup> The BaSi<sub>2</sub> grains of variant A dominate on the Si(001) substrate, meaning that the GBs consist mostly of BaSi<sub>2</sub>(001) planes. On the other hand, GBs running in the Si[1–10] direction seem roundish, and thereby several crystal planes or random GBs are likely to consist of the GBs. At present, we have not yet determined these crystal planes.

Figures 2(a) and 2(b) show the  $5 \times 5 \mu\text{m}^2$  AFM topographic and KFM electrostatic potential ( $\phi$ ) images, respectively, measured for sample A, BaSi<sub>2</sub> on Si(111), with their

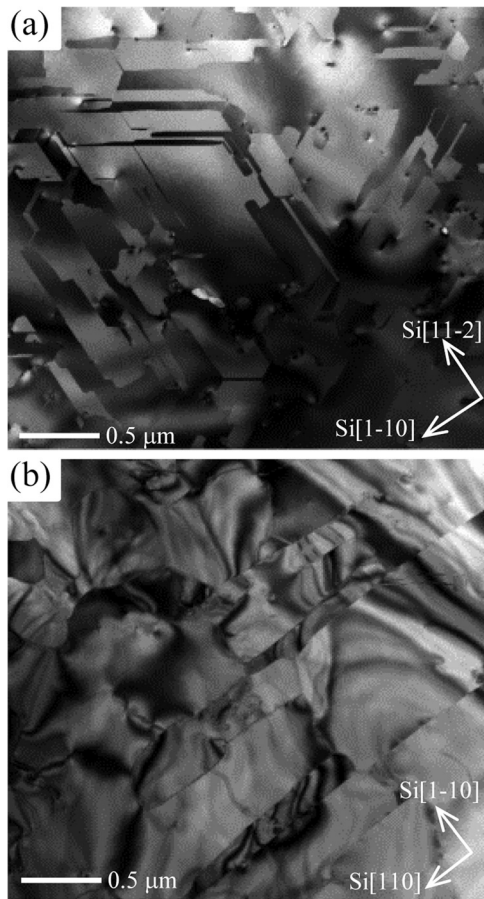


FIG. 1. Plan-view bright-field TEM images observed along near [100] zone axis of BaSi<sub>2</sub> for (a) BaSi<sub>2</sub> on Si(111) and (b) BaSi<sub>2</sub> on Si(001).

cross sectional profiles along the white lines in the same area. The positions of colored lines correspond to those of GBs in the cross sectional profiles in Figs. 2(a) and 2(b). We see that the electrostatic potentials at the GBs are higher than those in the grain. Since the energy band lineup is defined for negatively loaded electrons, the potential corresponds to the inversed work function divided by the elemental charge. This result means that band bending occurs downwards at the GBs as shown in Fig. 3(a). This is probably attributed to positively charged Ba atoms on the BaSi<sub>2</sub>(011)/(0-11) planes, which consist of these GBs. In a unit cell of BaSi<sub>2</sub>, there are 8 Ba and 16 Si atoms, the latter of which form Si<sub>4</sub> tetrahedra, and can be considered as Zintl anions.<sup>26</sup> Due to the difference in electronegativity between Ba and Si, Ba atoms are positively charged and the Si<sub>4</sub> tetrahedra is negatively charged in BaSi<sub>2</sub>. The BaSi<sub>2</sub>(011)/(0-11) planes consist of Ba atoms only, and thus they are considered positively charged. We speculate that's why the potentials become higher at the GBs than those in the grain interiors.

Figures 2(c) and 2(d) show the  $5 \times 5 \mu\text{m}^2$  AFM topographic and KFM electrostatic potential images, respectively, measured for sample B, BaSi<sub>2</sub> on Si(001). Their cross sectional profiles along the white lines in the same area are also shown. In the case of BaSi<sub>2</sub> grown on Si(001), one type of variant (variant A) was dominantly grown. We see that the BaSi<sub>2</sub> grains extend in the Si[110] direction in Fig. 2(c) as observed in the plan-view TEM image of Fig. 1(b).

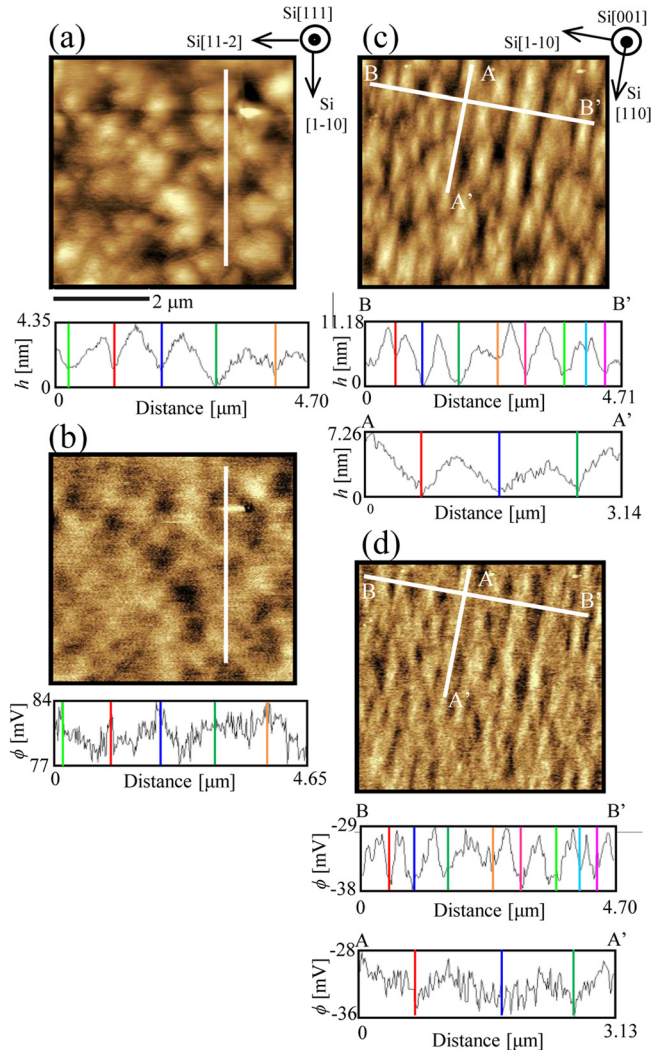


FIG. 2. (a) AFM topographic and (b) KFM electrostatic potential images with their cross sections along the white lines for sample A, undoped *n*-BaSi<sub>2</sub> on Si(111). (c) AFM topographic and (d) KFM electrostatic potential images with their cross sections along white lines AA', parallel to Si[110], and BB', parallel to Si[1-10], for sample B, undoped *n*-BaSi<sub>2</sub> on Si(001). The observed area is  $5 \times 5 \mu\text{m}^2$ .

Therefore, we investigated the electrostatic potentials along line AA', parallel to Si[110], and also along line BB', parallel to Si[1-10] because those GBs are composed of different planes. As shown in Fig. 2(d), the GBs have a lower electrostatic potential than the inner part of the grains, meaning that band bending occurs upwards at the GBs as shown in Fig. 3(b). The difference in the band bending at the GBs between BaSi<sub>2</sub>/Si(111) and BaSi<sub>2</sub>/Si(001) is attributed to the difference in the BaSi<sub>2</sub> planes which consist of GBs. GBs along line AA' are composed of BaSi<sub>2</sub>(001) planes. From the crystallographic point of view, only Si atoms exist on the BaSi<sub>2</sub>(001) plane. Thus, they are considered to be negatively charged because BaSi<sub>2</sub> is a Zintl phase. We speculate that's why the electrostatic potentials are lower at the GBs than those in the grain interiors. As for GBs along line BB', we don't have enough data to discuss with right now. We should note here that impurity contaminations can also cause potential variations around GBs. Impurity segregation to GBs have been extensively studied in poly crystalline Si.<sup>27-29</sup> Very recently, Tsurekawa *et al.* confirmed that the GBs in

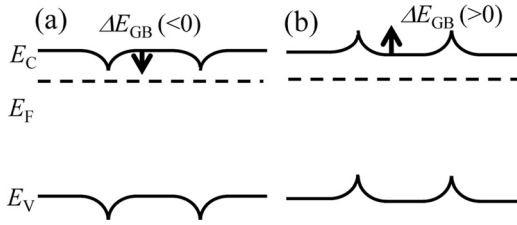


FIG. 3. Band lineups around GBs for (a) BaSi<sub>2</sub> on Si(111) and (b) BaSi<sub>2</sub> on Si(001).

Cu- and Fe-contaminated *p*-type Si cause a significant increase in the barrier height compared to non-contaminated Si.<sup>9</sup> We cannot exclude this possibility to explain the potential variations at the GBs of BaSi<sub>2</sub> films. There have been no reports so far on the segregation of impurities to GBs in BaSi<sub>2</sub>. Thus, detailed studies of impurity segregation in BaSi<sub>2</sub> are necessary in the near future.

Next, we evaluated the barrier height ΔE<sub>GB</sub> at GBs. To estimate ΔE<sub>GB</sub>, we used the following Eq. (1),

$$\Delta E_{\text{GB}} = -e(V_{\text{GB}} - V_{\text{G,ave}}), \quad (1)$$

where  $V_{\text{GB}}$  and  $V_{\text{G,ave}}$  are the electrostatic potential at GBs and the average potential of inner parts of two adjoining grains, respectively,  $e$  is the elementary charge. The same procedure was repeated 33 times for sample A. The histogram of barrier height is shown in Fig. 4(a). The barrier height for holes was positive and its absolute value ranges from 10 to 60 meV, and the average is approximately 30 meV. This value is almost the same as a thermal energy of 26 meV at room temperature (25 °C). The concave band structure at the GBs in the BaSi<sub>2</sub> on Si(111) is supposed to lead to repulsion of photogenerated holes (minority carriers) from the GBs, reducing the charge carrier recombination at the GBs. Therefore, the GBs do not work as recombination centers for minority carriers in the undoped *n*-BaSi<sub>2</sub>. This explains the long minority carrier diffusion length reaching 10 μm even for multi-domain epitaxial BaSi<sub>2</sub> films on Si(111).<sup>18</sup> The same analysis was performed for sample B, BaSi<sub>2</sub> on Si(001) along lines AA' and BB'. Figures 4(b) and 4(c) show the histograms of barrier height at GBs along Si[110] and Si[1-10], respectively. The barrier height for electrons was positive and ranges from 20 to 70 meV along Si[110], and from 20 to 45 meV along Si[1-10]. The averages are approximately 50 and 30 meV, respectively. The GBs have a convex band structure in the BaSi<sub>2</sub> on Si(001), attracting holes at the GBs. The average confinement energy for holes is as large as 50 meV at the GBs. If the Fermi level,  $E_{\text{F}}$ , at GBs lies on the GBs defect states in the band gap, the GBs are likely to work as recombination centers. Although we don't have data about the GB defect states at present, it is very important to discuss the position of  $E_{\text{F}}$  with respect to the bottom of the conduction band,  $E_{\text{C}}$ . The electron concentration of undoped *n*-type BaSi<sub>2</sub> is approximately  $5 \times 10^{15} \text{ cm}^{-3}$ .<sup>11</sup> Assuming that the effective density of states in the conduction band,  $N_{\text{C}}$ , is approximately  $2.6 \times 10^{19} \text{ cm}^{-3}$  from the principal-axis components of the effective-mass tensor for electrons,<sup>30</sup>  $E_{\text{F}}$  is located about 0.22 eV below  $E_{\text{C}}$  in the grain interiors at room temperature from the following Eq. (2),

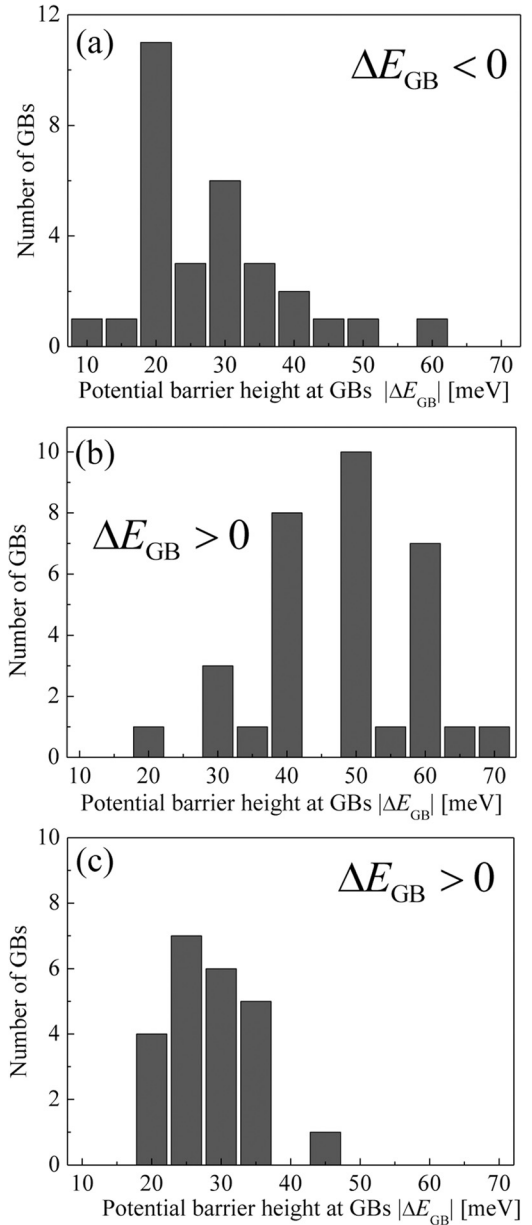


FIG. 4. Histograms of barrier height at GBs for (a) BaSi<sub>2</sub> on Si(111), (b) BaSi<sub>2</sub> on Si(001) along Si[110], and (c) that along Si[1-10].

$$E_{\text{C}} - E_{\text{F}} = kT \ln \left( \frac{N_{\text{C}}}{n} \right), \quad (2)$$

where  $k$  is the Boltzmann constant,  $T$  the absolute temperature, and  $n$  the electron concentration. In the case of BaSi<sub>2</sub>/Si(111), downward band bending occurred at the GBs and the average barrier height was approximately 30 meV. Therefore, the value of  $E_{\text{C}} - E_{\text{F}}$  is 0.19 eV at the GBs. On the other hand, upward band bending occurred at the GBs in the case of BaSi<sub>2</sub>/Si(001), and the average barrier height was approximately 50 meV and 30 meV along Si[110] and Si[1-10], respectively. Therefore, the value of  $E_{\text{C}} - E_{\text{F}}$  is approximately 0.25–0.27 eV at the GBs. If  $E_{\text{F}}$  at GBs is located around the GBs defect states, the GBs may function as recombination centers for photogenerated minority carriers in BaSi<sub>2</sub> films on Si(001).

In summary, we have evaluated the potential variations at the GBs in undoped *n*-BaSi<sub>2</sub> epitaxial films on Si(111) and

Si(001) applying KFM. The GBs had the concave band structure for BaSi<sub>2</sub>/Si(111), and the average barrier height was approximately 30 meV. This concave band structure may repulse holes. In contrast, the GBs have the convex band structure for BaSi<sub>2</sub>/Si(001). The average barrier height was approximately 50 meV along Si[110] and 30 meV along Si[1-10]. The origin of the difference was explained based on the crystal planes consisting of the GBs.

This work was financially supported by the Japan Science and Technology Agency (JST/CREST). TEM observations were conducted by Mr. N. Saitoh and Dr. N. Yoshizawa at the Electron Microscope Facility, supported in the IBEC Innovation Platform, AIST, Japan.

- <sup>1</sup>J. Kočka, A. Fejfar, H. Stuchlíková, J. Stuchlík, P. Fojtík, T. Mates, B. Rezek, K. Luterová, V. Švrček, and I. Pelant, *Sol. Energy Mater. Sol. Cells* **78**, 493 (2003).
- <sup>2</sup>C.-S. Jiang, R. Noufi, K. Ramanathan, J. A. AbuShama, H. R. Moutinho, and M. M. Al-Jassim, *Appl. Phys. Lett.* **85**, 2625 (2004).
- <sup>3</sup>J. Chen, T. Sekiguchi, D. Yang, F. Yin, K. Kido, and S. Tsurekawa, *J. Appl. Phys.* **96**, 5490 (2004).
- <sup>4</sup>M. Gloeckler, J. R. Sites, and W. K. Metzger, *J. Appl. Phys.* **98**, 113704 (2005).
- <sup>5</sup>S. Tsurekawa, K. Kido, and T. Watanabe, *Mater. Sci. Eng., A* **462**, 61 (2007).
- <sup>6</sup>M. Kawamura, T. Yamada, N. Suyama, A. Yamada, and M. Konagai, *Jpn. J. Appl. Phys. Part 1* **49**, 062301 (2010).
- <sup>7</sup>S. Oonishi, M. Kawamura, N. Takano, D. Hashimoto, A. Yamada, and M. Konagai, *Thin Solid Films* **519**, 7347 (2011).
- <sup>8</sup>T. Minemoto, Y. Wakisaka, and H. Takakura, *Jpn. J. Appl. Phys. Part 1* **50**, 031203 (2011).
- <sup>9</sup>S. Tsurekawa, H. Takahashi, Y. Nishibe, and T. Watanabe, *Philos. Mag.* **93**, 1413 (2013).
- <sup>10</sup>D. R. Kim, C. H. Lee, J. M. Weisse, I. S. Cho, and X. Zheng, *Nano Lett.* **12**, 6485 (2012).
- <sup>11</sup>K. Morita, Y. Inomata, and T. Suemasu, *Thin Solid Films* **508**, 363 (2006).
- <sup>12</sup>K. Toh, T. Saito, and T. Suemasu, *Jpn. J. Appl. Phys. Part 1* **50**, 068001 (2011).
- <sup>13</sup>W. Du, M. Suzuno, M. A. Khan, K. Toh, M. Baba, K. Nakamura, K. Toko, N. Usami, and T. Suemasu, *Appl. Phys. Lett.* **100**, 152114 (2012).
- <sup>14</sup>K. O. Hara, N. Usami, K. Toh, M. Baba, K. Toko, and T. Suemasu, *J. Appl. Phys.* **112**, 083108 (2012).
- <sup>15</sup>M. Kobayashi, Y. Matsumoto, Y. Ichikawa, D. Tsukada, and T. Suemasu, *Appl. Phys. Express* **1**, 051403 (2008).
- <sup>16</sup>M. A. Khan, K. O. Hara, W. Du, M. Baba, K. Nakamura, M. Suzuno, K. Toko, N. Usami, and T. Suemasu, *Appl. Phys. Lett.* **102**, 112107 (2013).
- <sup>17</sup>K. Nakamura, M. Baba, M. A. Khan, W. Du, M. Sasase, K. O. Hara, U. Usami, K. Toko, and T. Suemasu, *J. Appl. Phys.* **113**, 053511 (2013).
- <sup>18</sup>M. Baba, K. Toh, K. Toko, N. Saito, N. Yoshizawa, K. Jiptner, T. Sekiguchi, K. O. Hara, N. Usami, and T. Suemasu, *J. Cryst. Growth* **348**, 75 (2012).
- <sup>19</sup>Z. Zhang, X. Tang, O. Kiowski, M. Hetterich, U. Lemmer, M. Powalla, and H. Hölscher, *Appl. Phys. Lett.* **100**, 203903 (2012).
- <sup>20</sup>I. Visoly-Fisher, S. R. Cohen, and D. Cahen, *Appl. Phys. Lett.* **82**, 556 (2003).
- <sup>21</sup>S. Tsurekawa, K. Kido, and T. Watanabe, *Philos. Mag. Lett.* **85**, 41 (2005).
- <sup>22</sup>S. Honda, T. Mates, B. Rezek, A. Fejfar, and J. Kočka, *J. Non-Cryst. Solids* **354**, 2310 (2008).
- <sup>23</sup>Y. Inomata, T. Nakamura, T. Suemasu, and F. Hasegawa, *Jpn. J. Appl. Phys. Part 2* **43**, L478 (2004).
- <sup>24</sup>K. Toh, K. O. Hara, N. Usami, N. Saito, N. Yoshizawa, K. Toko, and T. Suemasu, *J. Cryst. Growth* **345**, 16 (2012).
- <sup>25</sup>K. Toh, K. O. Hara, N. Usami, N. Saito, N. Yoshizawa, K. Toko, and T. Suemasu, *Jpn. J. Appl. Phys. Part 1* **51**, 095501 (2012).
- <sup>26</sup>S. M. Kauzlarich, *Chemistry, Structure, and Bonding of Zintl Phases and Ions*, 1st ed. (Wiley-VCH, 1996).
- <sup>27</sup>A. Broniatowski, *Philos. Mag. B* **66**, 767 (1992).
- <sup>28</sup>R. Rizk and G. Nouet, *Interface Sci.* **4**, 303 (1997).
- <sup>29</sup>J. Chen, T. Sekiguchi, R. Xie, P. Ahmet, T. Chikyo, D. Yang, S. Ito, and F. Yin, *Scr. Mater.* **52**, 1211 (2005).
- <sup>30</sup>D. B. Migas, V. L. Shaposhnikov, and V. E. Borisenko, *Phys. Status Solidi B* **244**, 2611 (2007).